ISSN (Print) 1226-1750
ISSN (Online) 2233-6656
Journal of Magnetics 28(1), 38-48 (2023) https://doi.org/10.4283/JMAG.2023.28.1.038

Tilting Control of Rotor Suspended by Complex Magnetic Bearings with Coupling Torques

Jiqiang Tang[1,2]*, Min Zhang[1,2], Yupeng Li[1,2], and Jinji Sun[1,2]

[1]*School of Instrumentation and Optoelectronic Engineering, Beihang University, Beijing 100191, China*
[2]*Ningbo Institute of Technology, Beihang University, Ningbo 315800, China*

(Received 30 January 2023, Received in final form 17 March 2023, Accepted 28 March 2023)

For a novel Vernier-gimballing magnetically suspended flywheel (Vernier-gimballing MSFW) with conical magnetic bearing (MB) and Lorentz MB, the rotor's dynamic model is constructed based on the characteristics of both coupling torque generated by conical MB and nonlinear titling torques generated by Lorentz MB. To make the high-speeding rotor tilt precisely and fast to output large moment, the Vernier-gimballing control method based on the extended state observer (ESO) combined with feedback linearization is presented originally considering torques' complex nonlinearities, and the sliding mode control (SMC) with ESO is designed to improve the robustness of the closed-loop system. Simulations and experimental tests to verify the rightness and validity of SMC with ESO have been done and all research results indicate that the rotor can track the tilting signal faster and more accurately than classic SMC to output high precision moment.

Keywords : Vernier-gimballing magnetically suspended flywheel (Vernier-gimballing MSFW), Vernier-gimballing, Tilting, Sliding mode control (SMC), Extended state observer (ESO)

1. Introduction

For a high precision observation satellite, it is not only required that the satellite has features such as attitude maneuver, rapid stability, high precision orientation and so on to improve the maneuverability of the camera, but also required that the satellite has the ability to absorb the disturbing torques to ensure the stable imaging. To meet fully these space applications, the attitude control actuator is required to output large control moment and control the attitude of the satellite with high precision [1, 2]. The magnetically suspended flywheel (MSFW) is an important inertial actuator in a spacecraft's attitude control system by changing the rotor's rotatory speed to generate suitable attitude control moments [3, 4], but this control moment is generally too small to meet fully the maneuvering requirements [5]. As for the 5 degree-of-freedoms (DOFs) MSFW, it can not only generate a control moment around the rotor's rotary axis by changing its speed, but also generate control moment in other 2 DOFs by tilting actively the momentum vector with respect to the spacecraft body. This kind of MSFW named Vernier-gimballing MSFW [6-8] is possible to control the attitude of spacecraft by fewer needed flywheels. Being superior to other attitude actuators, the main features of Vernier-gimballing MSFW include the large outputting attitude control moment and wide control bandwidth, and it has promised to fulfill the requirements of both precision and maneuvers.

In one Vernier-gimballing MSFW as shown in Fig. 1 [8-10], the Lorentz force-type MBs are used to control the rotor's tilting, and a novel conical reluctance force-type MB is used to control the rotor's translation in 3 DOFs and to avoid common reluctance force-type MBs' forces coupling between different channels or large additional tilting torque when rotor is tilted. For a Vernier-gimballing MSFW with conical MB and Lorentz MB, the tilting control of high-speed rotor is essentially the rotor's tracking control in a complex nonlinear system due to its large tilting angle. Furthermore, the coupling torque between axial and radial direction inevitably is a complex nonlinear moment and related to many time-varying parameters, such as the current, translational displacement and tilting angle when the rotor's shaft is tilted accurately and fast.

*Corresponding author: Tel: +86-01082316813
Fax: +86-01082317396, e-mail: tjq_72@163.com

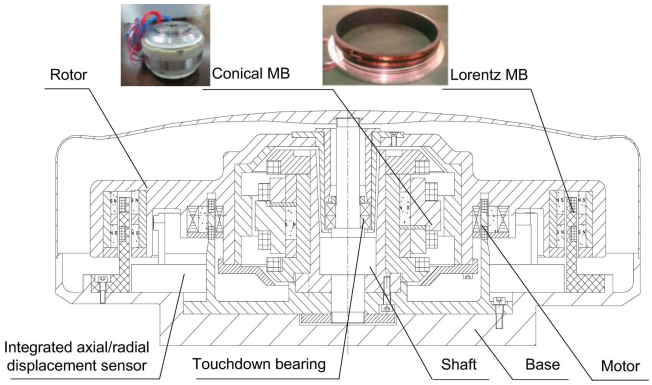

Fig. 1. (Color online) Vernier-gimballing MSFW with conical MB.

Considering these strong gyroscopic effects, the nonlinearity in MB-rotor system, the cross feedback control is widely used to ensure the rotor's stable suspension [11], and the linearization and decoupling (L&D) methods have become a popular control method to improve its precision. Wen *et al*. [12] decoupled the gyroscopic effects by L&D control method, Lin *et al.* [13] and Darbandi *et al.* [14] transformed the nonlinear MB-rotor system into a linear one through the input-output feedback linearization. Considering the complex multi-source disturbances and parameter uncertainties, Dong *et al.* [15] regulate the deviation of MB from its equilibrium position by adaptive back stepping controller and adaptive observer, but the adaptive control methods used usually for slowly changing uncertainties are not suitable to these uncertainties changing rapidly in rotor's tracking control. To suppress disturbance, there are many methods such as robust control method, compensation control method and so on. Among of these, the SMC method is an effective robust control method, but the nonlinear switch function in classic SMC will result in chattering generally [16]. Lee *et al.* [17] replaced the sign function in SMC by saturation one to reduce this chattering while the static error determined by the selected boundary layer's thickness was introduced unavoidably. Because only SMC method cannot achieve the MB-rotor system's high precision control, Grochmal *et al.* [18] designed a reduced-order disturbance observer as a compensation method to estimate the disturbance affecting the tracking of rotor's shaft suspended by magnetic bearings. Yu *et al.* [19] employed a disturbance observer to suppress the synchronous disturbance in MSFW based on an established accurately synchronous disturbance model. However, this disturbance observer relies on the disturbance accurate model and is not suitable for Vernier-gimballing MSFW with complex coupling torques. The extended state observer (ESO) proposed by Han and divided into nonlinear ESO and the linear ESO can accurately estimate the disturbance acting on the system without disturbance models [20]. Compared to the linear ESO, the nonlinear one requires smaller gains and usually displays better performance, but the gains are harder to select. Xu *et al.* [21] researched a linear ESO in MB-rotor system for a flywheel to estimate the external disturbance and designed a robust controller to compensate it, many researchers studied additional linear ESO to improve the robustness due to the linear ESO's poor static-state performance [22-23].

Besides the strong gyroscopic effects, the coupling torques and nonlinear magnetic moments affect the performance of Vernier-gimballing MSFW seriously. With respect to these coupling torques generated by conical MB, this paper emphasizes on the analysis of these factors and the tilting control method and research the feedback linearization and ESO deeply to estimate the coupling torques. A new control method of SMC with ESO is proposed originally to compensate the observed disturbance and improve the robustness of the system and series of simulations and experimental tests have been done to verify its rightness and validity.

2. Rotor's Dynamic Modeling

In this Vernier-gimballing MSFW, the conical MB located in the center of the flywheel is used to control rotor's translations in axial and radial directions, the Lorentz MB arranged in the outer rim of rotor is used to tilt rotor around X and Y-axis to generate large control moment. When the rotor is suspended stably in the central position, as shown in Fig. 2(a), the radial suspension force generated by conical MB in left side F_{rx+} equals to that in right side F_{rx-}, but their directions are inverse. The summation of axial suspension force $F_{az\text{-}up}$ at upper end and $F_{az\text{-}lo}$ at lower one for conical MB equals to the rotor's weight. When the rotor is tilted, a large moment will be generated due to the gyroscope effect of high-speed rotor.

As shown in Fig. 2(b), the angle between conical surface and central axis is θ, these designed conical acting arms are L_r and L_a, respectively. When the rotor is tilted by β around Y-axis, these forces generated by the conical MB from down to up represented by F_{dx-}, F_{dx+}, F_{ux-} and F_{ux+}; Similarly, these forces can also be represented by F_{dx+}, F_{dy+}, F_{uy-} and F_{uy+} when the rotor is tilted by α around X-axis. Due to limitations of conical MB's volume and height, it is impossible for all forces to be aligned with its centroid, then the additional magnetic forces and torques do exist in the tilting channel. Defined

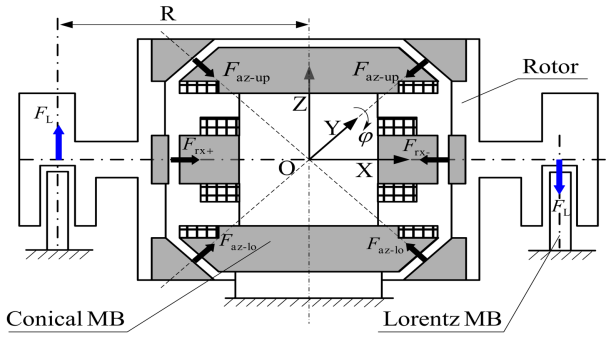

(a) Forces generated by conical MB in ideal situation

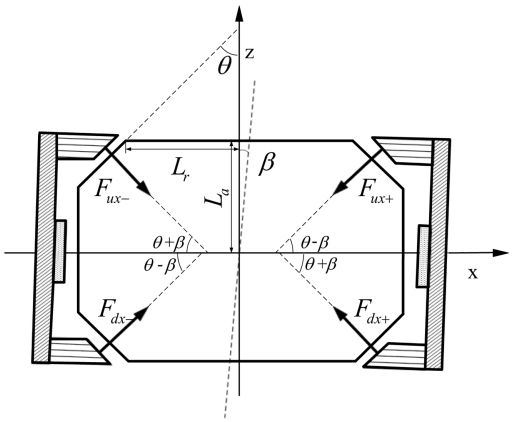

(b) Forces generated by conical MB in actual situation

Fig. 2. (Color online) Forces generated by conical MB in ideal situation and actual situation.

F_{az} as the effective axial control force, F_{rx} and F_{ry} as these disturbing forces in these radial channels, respectively, the forces generated by the conical magnetic pole without translational displacements along three axes can be expressed as following

$$\begin{cases} F_{rx}=\left[\left(F_{ux-}+F_{dx-}\right)-\left(F_{ux+}+F_{dx+}\right)\right]\cos\theta \\ F_{ry}=\left[\left(F_{uy-}+F_{dy-}\right)-\left(F_{uy+}+F_{dy+}\right)\right]\cos\theta \\ F_{az}=\left[\left(F_{dx+}+F_{dx-}+F_{dy+}+F_{dy-}\right)-\left(F_{ux+}+F_{ux-}+F_{uy+}+F_{uy-}\right)\right]\sin\theta \end{cases} \tag{1}$$

Set k_i and k_x as conical MB's current stiffness and displacement one, Δx as rotor's translational displacement, respectively, then

$$F_{dx-}=k_i i+k_x\left(x+\Delta x\right) \tag{2}$$

Similarly, F_{dx+}, F_{ux-}, F_{ux+}, F_{dy-}, F_{dy+}, F_{uy-} and F_{uy+} can also be expressed as the same forms.

The coupling torques generated by the conical MB are as follows

$$\begin{cases} T_{rx}=\left(F_{uy+}+F_{dy-}\right)\left[L_a\cos\left(\theta-\beta\right)-L_r\sin\left(\theta-\beta\right)\right] \\ \quad +\left(F_{uy-}+F_{dy+}\right)\left[L_r\sin\left(\theta+\beta\right)-L_a\cos\left(\theta+\beta\right)\right] \\ T_{ry}=\left(F_{ux-}+F_{dx+}\right)\left[L_a\cos\left(\theta+\beta\right)-L_r\sin\left(\theta+\beta\right)\right] \\ \quad +\left(F_{ux+}+F_{dx-}\right)\left[L_r\sin\left(\theta-\beta\right)-L_a\cos\left(\theta-\beta\right)\right] \end{cases} \tag{3}$$

From (1) and (3), we can find out that the conical magnetic pole generate not only the effective axial control force F_{az}, but also some disturbing forces F_{rx} or F_{ry} and coupling torques T_{rx} or T_{ry} in radial directions. It is obvious that these coupling torques T_{rx} and T_{ry} are complex nonlinear related to translational displacements, tilting angles and coil currents even though the conical acting arms L_r and L_a are less than those of a common MB by far. These coupling torques are hard to be expressed accurately and generally simplified when the rotor is tilted, so the precision of tilting control and output torque for the Vernier-gimballing MSFW will be affected seriously. For example, the finite element analysis shows that the coupling torque is up to 0.55 Nm and the output torque is 1.1Nm when the rotor's tilting angle is up to 1°, and the precision of tilting control and output torque will be affected urgently if the coupling torque is ignored.

Two pairs of coils (there are four sets of coils totally) in the Lorenz MB are used to control the tilting motion around X-axis or Y-axis. When the coils are electrified, either one two sets of coils controlling the tilting around the Y-axis or another two sets of coils controlling the tilting around the X-axis will generate the magnetic force up and down along the Z-axis, respectively. As illustrated in Fig. 3, if the turns of the coil winding is N, the magnetic flux density in the gap is B, the coil current and effective length of the coil are I_{cu} and L, and the radius of the bearing's stator is L_d, respectively, the magnetic force is as follows

$$F_{Lx-}=F_{Lx+}=NBI_{cu}L \tag{4}$$

And the generated effective torque to control rotor's tilting around Y-axis or X-axis is

$$\begin{cases} T_y=\left(F_{Lx-}+F_{Lx+}\right)L_d=\left(2NBI_\beta L\right)L_d=k_\beta I_\beta \\ T_x=\left(F_{Ly-}+F_{Ly+}\right)L_d=\left(2NBI_\alpha L\right)L_d=k_\alpha I_\alpha \end{cases} \tag{5}$$

where k_α and k_β are these moment stiffness coefficients of Lorenz MB around X-axis and Y-axis, respectively (Nm/A), I_α and I_β are the control currents in X-axis and Y-axis channels of Lorentz MB (A).

Because the magnetic density in the middle of axial gap is maximum and gradually decreases along the axial gap, this tilting torques are nonlinear, and can be expressed as

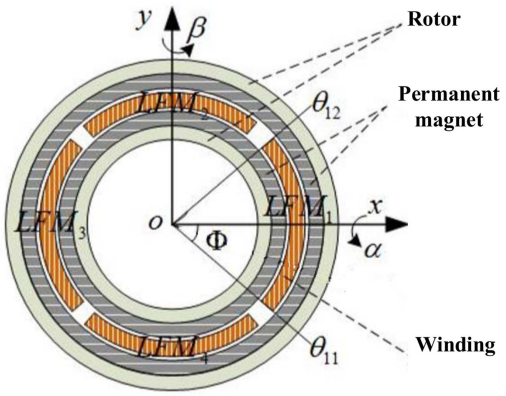

(a) End view

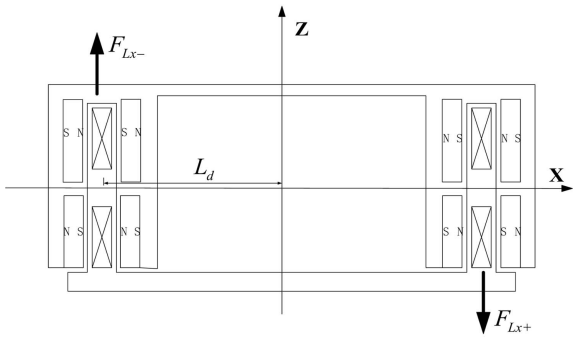

(b) Sectional view

Fig. 3. (Color online) Schematic diagram of Lorenz MB.

$$\boldsymbol{T}_{\mathrm{l}}=\begin{bmatrix} f_{\alpha}(\alpha,\beta)I_{\alpha} \\ f_{\beta}(\alpha,\beta)I_{\beta} \end{bmatrix}=\begin{bmatrix} k_{\alpha}I_{\alpha} \\ k_{\beta}I_{\beta} \end{bmatrix}=\boldsymbol{K}(\alpha,\beta)\boldsymbol{I}_{\mathrm{l}} \tag{6}$$

where $\mathbf{K}(\alpha, \beta)$ is the time variable current stiffness matrix related to tilting angle α and β.

Eq. (6) can be rewritten as

$$\boldsymbol{T}_{\mathrm{l}}=(\boldsymbol{K}_{\mathrm{i}}+\Delta\boldsymbol{K}_{\mathrm{i}})\boldsymbol{I}_{\mathrm{l}} \tag{7}$$

where $\boldsymbol{K}_{\mathrm{i}}$ is the nominal stiffness matrix, and $\boldsymbol{K}_{\mathrm{i}} = [k_{\alpha}, k_{\beta}]^{\mathrm{T}}$, $\Delta\boldsymbol{K}_{\mathrm{i}}$ is the model error matrix, and $\Delta\boldsymbol{K}_{\mathrm{i}} = [\Delta k_{\alpha}, \Delta k_{\beta}]^{\mathrm{T}}$.

For the rotor in Vernier-gimballing MSFW, its inertial moments around X-axis, Y-axis and Z-axis are represented by J_{x}, J_{y} and J_{z}, respectively; Ω is the rotor's rotary speed, then the dynamic equations with the existence of disturbances d_{α} and d_{β} can be expressed as following

$$\begin{cases} J_{\mathrm{x}}\ddot{\alpha}+J_{\mathrm{z}}\Omega\dot{\beta}=k_{\alpha}I_{\alpha}+d_{\alpha} \\ J_{\mathrm{y}}\ddot{\beta}-J_{\mathrm{z}}\Omega\dot{\alpha}=k_{\beta}I_{\beta}+d_{\beta} \end{cases} \tag{8}$$

Considering the coupling torques generated by conical MB as expressed in (3) and the time variable current stiffness of Lorentz MB as expressed in (7), Eq. (8) can be expressed as

$$\begin{cases} J_{\mathrm{x}}\ddot{\alpha}+J_{\mathrm{z}}\Omega\dot{\beta}=(k_{\alpha}+\Delta k_{\alpha})I_{\alpha}+T_{\mathrm{rx}} \\ J_{\mathrm{y}}\ddot{\beta}-J_{\mathrm{z}}\Omega\dot{\alpha}=(k_{\beta}+\Delta k_{\beta})I_{\beta}+T_{\mathrm{ry}} \end{cases} \tag{9}$$

From (9), we can find out that both the coupling torques and their nonlinearity cannot be ignored to control the high-speed rotor tilting with high precision.

3. Tilting controller design

3.1. State feedback linearization of tilting motion

To design the rotor's titling control method, we need to transform (8) into standard state equation by defining state variables $\boldsymbol{x}_{\alpha\beta}$ as $[x_{\mathrm{t1}}, x_{\mathrm{t2}}, x_{\mathrm{t3}}, x_{\mathrm{t4}}]^{\mathrm{T}} = [\alpha, \beta, \dot{\alpha}, \dot{\beta}]^{\mathrm{T}}$, input variables $\boldsymbol{u}_{\alpha\beta}$ as $[u_{\alpha}, u_{\beta}]^{\mathrm{T}} = [I_{\alpha}, I_{\beta}]^{\mathrm{T}}$ and output variables $\boldsymbol{y}_{\alpha\beta}$ as $[y_{\alpha}, y_{\beta}]^{\mathrm{T}} = [\alpha, \beta]^{\mathrm{T}}$

$$\begin{cases} \dot{\boldsymbol{x}}_{\alpha\beta}=\boldsymbol{f}(x_{\alpha\beta})+\boldsymbol{g}(x_{\alpha\beta})\boldsymbol{u}_{\alpha\beta}+\boldsymbol{d}(x_{\alpha\beta}) \\ \boldsymbol{y}_{\alpha\beta}=\boldsymbol{h}(x_{\alpha\beta}) \end{cases} \tag{10}$$

where $\boldsymbol{f}(x_{\alpha\beta}) = [x_{\mathrm{t3}}, x_{\mathrm{t4}}, -J_{\mathrm{z}}\Omega x_{\mathrm{t4}}/J_{\mathrm{x}}, J_{\mathrm{z}}\Omega x_{\mathrm{t3}}/J_{\mathrm{y}}]^{\mathrm{T}}$,

$$\boldsymbol{g}(x_{\alpha\beta})=\begin{bmatrix} g_1 \\ g_2 \end{bmatrix}^{\mathrm{T}}=\begin{bmatrix} 0,0,k_{\alpha}/J_{\mathrm{x}},0 \\ 0,0,0,k_{\beta}/J_{\mathrm{y}} \end{bmatrix}^{\mathrm{T}},$$

$$\boldsymbol{h}(x_{\alpha\beta})=[h_1(x_{\alpha\beta})\ h_2(x_{\alpha\beta})]^{\mathrm{T}}=[x_{\mathrm{t1}}\ x_{\mathrm{t2}}]^{\mathrm{T}},$$

$$\boldsymbol{d}(x_{\alpha\beta})=[0,0,d_1,d_2]^{\mathrm{T}}=[0,0,d_{\alpha}/J_{\mathrm{x}},d_{\beta}/J_{\mathrm{y}}]^{\mathrm{T}}.$$

According to the differential geometry theory [24], the Lee derivative of $h(x)$ alongside field $f(x)$ can be defined as

$$L_{f(x)}h(x)=(\partial h(x)/\partial x^{\mathrm{T}})f(x) \tag{11}$$

Applying (11) to the tilting motion, the following equations are satisfied

$$L_{\boldsymbol{g}(x_{\alpha\beta})}\boldsymbol{h}(x_{\alpha\beta})=0 \tag{12}$$

$$L_{\boldsymbol{g}(x_{\alpha\beta})}L_{f(x_{\alpha\beta})}\boldsymbol{h}(x_{\alpha\beta})=\begin{bmatrix} k_{\alpha}/J_{\mathrm{x}} & 0 \\ 0 & k_{\beta}/J_{\mathrm{y}} \end{bmatrix}\neq 0 \tag{13}$$

Therefore, both the relative orders r_{x} of the X-axis control channel and that r_{y} of Y-axis control channel are $r_{\mathrm{x}} = r_{\mathrm{y}} = 2$, and the sum of r_{x} and r_{y} equals to the system's state variable dimension, the rotor's tilting in Vernier-gimballing MSFW satisfies the state feedback linearization condition, and (10) can be transformed into a linear system.

The state variables of this system is selected as

$$\boldsymbol{z}=\begin{bmatrix} z_{11} \\ z_{12} \\ z_{21} \\ z_{22} \end{bmatrix}=\begin{bmatrix} L_f^0 h_1\left(x_{\alpha\beta}\right) \\ L_f^1 h_1\left(x_{\alpha\beta}\right) \\ L_f^0 h_2\left(x_{\alpha\beta}\right) \\ L_f^1 h_2\left(x_{\alpha\beta}\right) \end{bmatrix}=\begin{bmatrix} x_{t1} \\ x_{t2} \\ x_{t3} \\ x_{t4} \end{bmatrix} \tag{14}$$

Defined matrix

$$\boldsymbol{A}(x)=\begin{bmatrix} L_{g1}L_f h_1\left(x_{\alpha\beta}\right) & L_{g2}L_f h_1\left(x_{\alpha\beta}\right) \\ L_{g1}L_f h_2\left(x_{\alpha\beta}\right) & L_{g2}L_f h_2\left(x_{\alpha\beta}\right) \end{bmatrix}=\begin{bmatrix} k_\alpha / J_{\mathrm{x}} & 0 \\ 0 & k_\beta / J_{\mathrm{y}} \end{bmatrix},$$

and matrix $\boldsymbol{B}(x)=\begin{bmatrix} L_f^2 h_1\left(x_{\alpha\beta}\right) \\ L_f^2 h_2\left(x_{\alpha\beta}\right) \end{bmatrix}=\begin{bmatrix} -J_{\mathrm{z}}\Omega x_{t4} / J_{\mathrm{x}} \\ J_{\mathrm{z}}\Omega x_{t3} / J_{\mathrm{y}} \end{bmatrix}$, a new state variable **v** with virtual control variables ν_1 and ν_2 can be defined as

$$\boldsymbol{v}=\begin{bmatrix} \nu_1 & \nu_2 \end{bmatrix}^{\mathrm{T}}=\boldsymbol{B}(x)+\boldsymbol{A}(x)\left[u_1,u_2\right]^{\mathrm{T}} \tag{15}$$

Since the matrix $\boldsymbol{A}(x)$ is reversible, the following state feedback control law $\boldsymbol{u}$ can be designed as

$$\boldsymbol{u}=\left[u_1,u_2\right]^{\mathrm{T}}=\boldsymbol{A}^{-1}(x)\left[-\boldsymbol{B}(x)+\boldsymbol{v}\right] \tag{16}$$

Therefore, the multi-input and multi-output system is decoupled into a two independent linear systems as follows

$$\begin{cases} \begin{bmatrix} \dot{z}_{11} \\ \dot{z}_{12} \end{bmatrix}=\begin{bmatrix} 0 & 1 \\ 0 & 0 \end{bmatrix}\begin{bmatrix} z_{11} \\ z_{12} \end{bmatrix}+\begin{bmatrix} 0 \\ \nu_1 \end{bmatrix}+\begin{bmatrix} 0 \\ d_1 \end{bmatrix} \\ \begin{bmatrix} \dot{z}_{21} \\ \dot{z}_{22} \end{bmatrix}=\begin{bmatrix} 0 & 1 \\ 0 & 0 \end{bmatrix}\begin{bmatrix} z_{21} \\ z_{22} \end{bmatrix}+\begin{bmatrix} 0 \\ \nu_2 \end{bmatrix}+\begin{bmatrix} 0 \\ d_2 \end{bmatrix} \end{cases} \tag{17}$$

The differential geometric coordinate transformation and feedback linearization do not change the controllability of the system, and it can be seen from (17) that the system is completely controllable.

3.2. Extended state observer (ESO) design

Since the complex coupling torques cannot be modelled accurately, an ESO is designed to observe these disturbances. After state feedback linearization, the tilting dynamic model is turned into an integral cascaded linear system as

$$\begin{cases} \dot{\boldsymbol{x}}_1=\boldsymbol{x}_2 \\ \dot{\boldsymbol{x}}_2=\boldsymbol{v}+\boldsymbol{d}(t) \\ \boldsymbol{y}=\boldsymbol{x}_1 \end{cases} \tag{18}$$

where $\boldsymbol{x}_1=\left[\alpha,\beta\right]^{\mathrm{T}}$, $\boldsymbol{v}=\left[\nu_1,\nu_2\right]^{\mathrm{T}}$ is the input of the linear system, and $\boldsymbol{d}(t)=\left[d_\alpha / J_{\mathrm{x}}, d_\beta / J_{\mathrm{y}}\right]^{\mathrm{T}}$.

Set $\boldsymbol{w}(t)$ as the derivative of the coupling torques $\boldsymbol{d}(t)$ and extend $\boldsymbol{d}(t)$ as a new state variable $\boldsymbol{x}_3$, then (18) is extended to be

$$\begin{cases} \dot{\boldsymbol{x}}_1=\boldsymbol{x}_2 \\ \dot{\boldsymbol{x}}_2=\boldsymbol{v}+\boldsymbol{x}_3 \\ \dot{\boldsymbol{x}}_3=\boldsymbol{w}(t) \\ \boldsymbol{y}=\boldsymbol{x}_1 \end{cases} \tag{19}$$

Defined $\boldsymbol{z}_1$, $\boldsymbol{z}_2$ and $\boldsymbol{z}_3$ as the estimations of $\boldsymbol{x}_1$, $\boldsymbol{x}_2$ and $\boldsymbol{x}_3$, and the related estimation error of $\boldsymbol{x}_1$ is $\boldsymbol{e}_1=\boldsymbol{z}_1-\boldsymbol{x}_1$, then the ESO can be designed as

$$\begin{cases} \dot{\boldsymbol{z}}_1=\boldsymbol{z}_2-\beta_{01}\boldsymbol{e}_1 \\ \dot{\boldsymbol{z}}_2=\boldsymbol{z}_3-\beta_{02}\boldsymbol{e}_1+\boldsymbol{v} \\ \dot{\boldsymbol{z}}_3=-\beta_{03}\boldsymbol{e}_1 \end{cases} \tag{20}$$

where β_{01}, β_{02} and β_{03} are the gain coefficients of ESO.

Defined the related estimation error of $\boldsymbol{x}_2$ as $\boldsymbol{e}_2=\boldsymbol{z}_2-\boldsymbol{x}_2$, and that of $\boldsymbol{x}_3$ as $\boldsymbol{e}_3=\boldsymbol{z}_3-\boldsymbol{x}_3$, then the error dynamics of ESO can be obtained by subtracting (19) from (20)

$$\begin{cases} \dot{\boldsymbol{e}}_1=\boldsymbol{e}_2-\beta_{01}\boldsymbol{e}_1 \\ \dot{\boldsymbol{e}}_2=\boldsymbol{e}_3-\beta_{02}\boldsymbol{e}_1 \\ \dot{\boldsymbol{e}}_3=-\boldsymbol{w}(t)-\beta_{03}\boldsymbol{e}_1 \end{cases} \tag{21}$$

To describe the characteristic equation of the estimation errors, Eq. (21) can be rewritten as

$$\begin{pmatrix} \dot{\boldsymbol{e}}_1 \\ \dot{\boldsymbol{e}}_2 \\ \dot{\boldsymbol{e}}_3 \end{pmatrix}=\begin{pmatrix} -\beta_{01} & 1 & 0 \\ -\beta_{02} & 0 & 1 \\ -\beta_{03} & 0 & 0 \end{pmatrix}\begin{pmatrix} \boldsymbol{e}_1 \\ \boldsymbol{e}_2 \\ \boldsymbol{e}_1 \end{pmatrix}+\begin{pmatrix} 0 \\ 0 \\ -\boldsymbol{w}(t) \end{pmatrix}=\boldsymbol{L}\begin{pmatrix} \boldsymbol{e}_1 \\ \boldsymbol{e}_2 \\ \boldsymbol{e}_1 \end{pmatrix}+\begin{pmatrix} 0 \\ 0 \\ -\boldsymbol{w}(t) \end{pmatrix} \tag{22}$$

Then we can obtain the following equation

$$\left|\lambda\boldsymbol{I}-\boldsymbol{L}\right|=\lambda^3+\beta_{01}\lambda^2+\beta_{02}\lambda+\beta_{03}=0 \tag{23}$$

Based on the classical control theory, Eq. (22) is stable when the characteristic equation (23) satisfies the Hurwitz condition. If the gains of ESO are positive, the roots of (23) will have negative real parts.

To have a good transition process and a stable dynamic process, the characteristic equation (23) is usually set as following when the bandwidth of ESO is ω_0.

$$\left(\lambda+\omega_0\right)^3=0 \tag{24}$$

For a Vernier-gimballing MSFW with system bandwidth ω_{c}, generally $\omega_0=(3\sim5)\omega_{\mathrm{c}}$, the gains of ESO can be designed as

$$\beta_{01}=3\omega_0,\ \beta_{02}=3\omega_0^2,\ \beta_{03}=\omega_0^3 \tag{25}$$

3.3. Sliding mode controller

For Lorentz MB, the magnetic flux density is uneven in the gap between internal and external magnets, the

current stiffness is time variable and its moment is nonlinear. For a MB-rotor system in Vernier-gimballing MSFW, there are some uncertainties such as the dynamic modelling error, it is necessary to design a controller to improve its robustness. Here the SMC method introduced to the feedback linearization model is used to deal with these uncertainties.

For these titling angles α and β with expected values α_0 and β_0, respectively, their relative error $\delta_1 = \alpha - \alpha_0$ and $\delta_2 = \beta - \beta_0$. For a certain coefficient c, the sliding mode functions for X-axis control channel is designed as $s_1 = c\delta_1 + \dot{\delta}_1$, and that for Y-axis control channel is designed as $s_2 = c\delta_2 + \dot{\delta}_2$.

To approach the SMC law $\boldsymbol{u}_{\text{com}}$ for this system, the approach law is designed as $\dot{s} = -\eta sgn(s)$ with matrix $\boldsymbol{C}(x) = \left[-\eta sgn(s_1), -\eta sgn(s_2)\right]^{\text{T}}$, and the observed coupling torques matrix $\hat{\boldsymbol{d}}(x)$ by ESO is defined as $\hat{\boldsymbol{d}}(x) = \left[\hat{d}_1, \hat{d}_2\right]^{\text{T}}$, and then $\boldsymbol{u}_{\text{com}}$ is as follows

$$\boldsymbol{u}_{\text{com}} = \boldsymbol{A}^{-1}(x)\left[-\boldsymbol{B}(x) + \boldsymbol{v} + \boldsymbol{C}(x) - \hat{\boldsymbol{d}}(x)\right] \tag{26}$$

Because these control algorithms for X-axis channel and Y-axis channel are same, here we only take that for X-axis channel as an example to show how to design it. Considering (15), $v_1 = \ddot{\alpha}_0 - c\dot{\delta}_1$, the Lyapunov function is described as $V = s_1^2/2$, then the derivative of V can be obtained as

$$\begin{aligned}\dot{V} = s_1\left(c\dot{\delta}_1 + \ddot{\delta}_2\right) = s_1\left(v_1 + d_1 - \eta\,\text{sgn}(s_1) - \hat{d}_1 - \ddot{\alpha}_0 + c\dot{\delta}_1\right) = \\ \left(d_1 - \hat{d}_1\right)s_1 - \eta|s_1| = s_1 e_d - \eta|s_1|\end{aligned} \tag{27}$$

where e_d is the error of the observed coupling torque by ESO.

If $e_{\max} \geq |e_d|$ and $\eta \geq e_{\max}$, the following equation will be obtained

$$\dot{V} \leq \left(e_{\max} - \eta\right)|s_1| \leq 0 \tag{28}$$

Eq. (28) verifies the stability of the designed tilting controller of the Vernier-gimballing MSFW, and the designed controller is illustrated in Fig. 4.

4. Simulations and Experimental Tests

To verify the performances of the proposed SMC with ESO method on controlling rotor's tilting, simulation and experimental research have been done with experimental setup as shown in Fig. 5, its main parameters are listed in Table 1. The angular momentum of this MSFW is 68

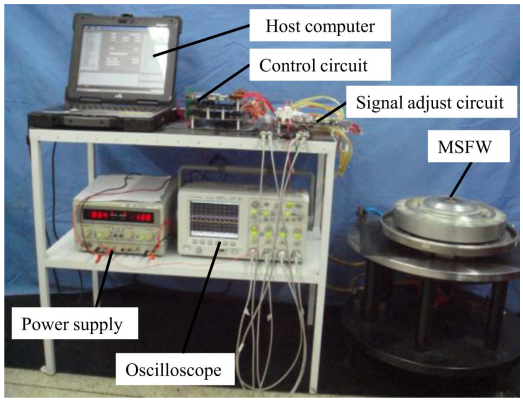

Fig. 5. (Color online) Experimental setup with Vernier-gimballing MSFW.

Table 1. Parameters of the system and controller.

Parameter	Value
J_z	0.148 kg.m^2
J_x, J_y	0.0737 kg.m^2
Ω	5000 r/min
η	3
c	20
β_{01}	1400
β_{02}	6.9×10^5
β_{03}	1.1×10^8

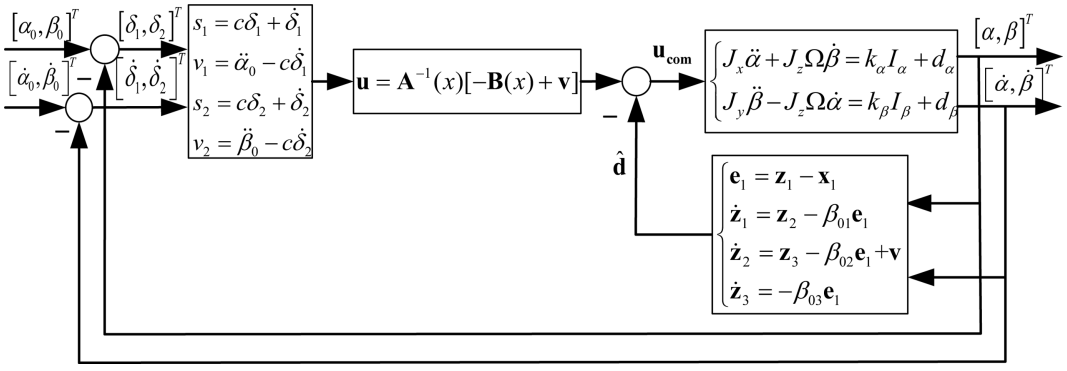

Fig. 4. Block diagram of SMC with ESO.

Nms, the rotor's working speed range varies from −5000 rpm to 5000 rpm, and the rotor's maximum radial tilting angle is 1.7°. The time variable current stiffness along X-axis is assumed as $4.44-29178\alpha^3-44.4\beta^2$ to simulate the system's uncertainty, and the expected tilting angle is assumed as harmonic signal or step signal with respect to different applications such as satellite's periodic disturbance suppression or satellite's reorientation. Because the results of rotor tilting around X-axis are same as that around Y-axis, here we only give these simulations and experimental results of rotor tilting around X-axis.

4.1. Simulations

To verify the effectiveness of ESO, its performances are depicted in Fig. 6(a) when the rotor's tilting angle is harmonic signal $0.1\sin 4\pi t$ and that are shown in Fig. 6(b) when the tilting angles is step signal $0.318\arctan 20t$, respectively. The reference disturbance represented by black dashed dot lines in Fig. 6(a) is $100\alpha^3-2\beta^2$ and that in Fig. 6(b) is $10\alpha^3-2\beta^2$, the red dotted lines represent the observed disturbance. The error of observed disturbance shown in Fig. 6(a) is about 0.003 Nm when the time is 0.56s and that in Fig. 6(b) is near 5×10^{-5} Nm when the time is 2.19s. It is clear that the ESO can estimate the reference disturbance accurately at beginning immediately, and the ESO can observe accurately this disturbance acting on the system with advantage of fast response.

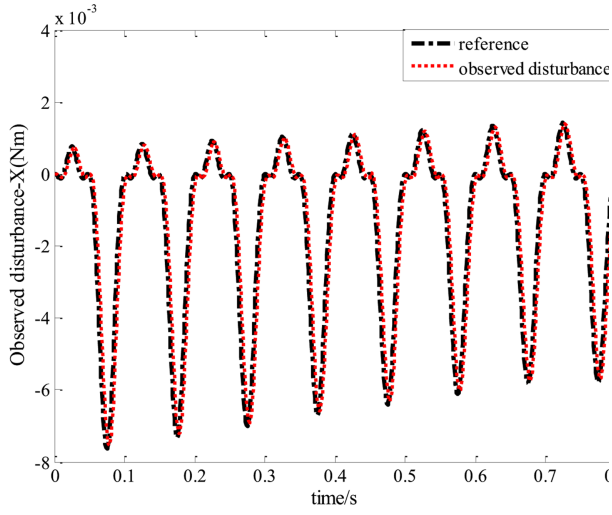

(a) Disturbance as harmonic signal

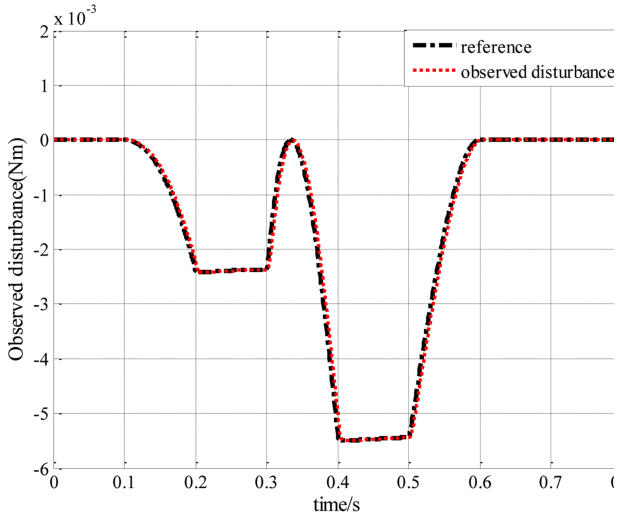

(b) Disturbance as step signal

Fig. 6. (Color online) Observed disturbance along X-axis.

To analyze the influence of coefficient c in sliding mode function on the performance of the proposed SMC with ESO, the accuracy and response time of tilting control are depicted in Fig. 7. Where the black dashed dot line represents the ideal angle or angular velocity, respectively, the green dotted one, the blue dashed one and the red solid one represents these results when $c=20$, $c=10c$ and $c=50c$, respectively. The dynamic response of tilting angle and its tracking error are depicted in Fig. 7(a) and (b), we can found out that the inputting signal can be tracked in all cases, and the tracking performance becomes better when the parameter c increases. The regulation time is shortest when $c=1000$ but its performance is improved limitedly when c increases from $10c$ to $50c$, and the partial enlarged drawings in Fig. 7(b) indicate that the steady error is reduced when parameter c increases while the jittering amplitude at steady state is same approximately when $c=10c$ and $c=50c$. The dynamic response of tilting velocity and tracking error are depicted in Fig. 7(c) and (d), we can found out that the inputting signal of tilting velocity can be tracked stably in three cases. The regulation time is short when $c=10c$ and $c=50c$, and the partial enlarged drawings Fig. 7(d) indicate that the jittering amplitude at steady state is the smallest when $c=10c$ and that is the largest when $c=50c$. From Fig. 7, we can draw a conclusion that the tilting control has better performance with merits of high precision and fast response when the coefficient c in sliding mode function has a suitable value.

Because the classic SMC (without ESO) is an effective robust control method to suppress disturbance and usually used in practice even if there is inevitably chattering resulted from its nonlinear switch function. To demonstrate the performance of the proposed SMC with ESO by comparison, the comparative simulations between SMC with ESO and classic SMC with same coefficients $c=200$ have been done and the main results are depicted

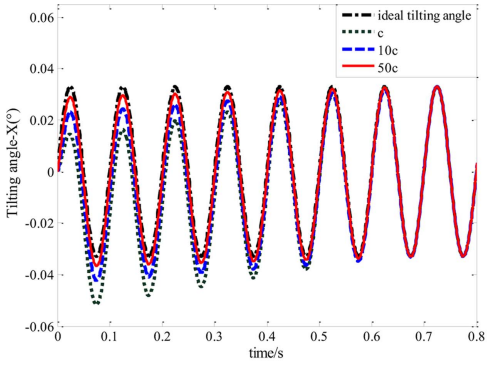

(a) Dynamic response of tilting angle

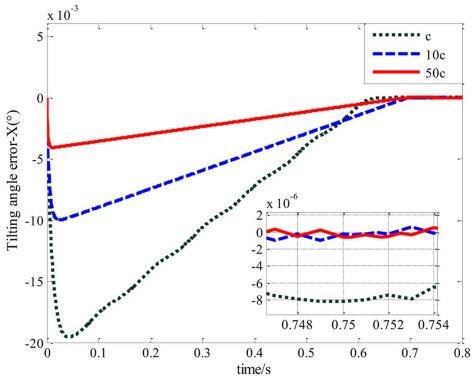

(b) Tracking error of tilting angle

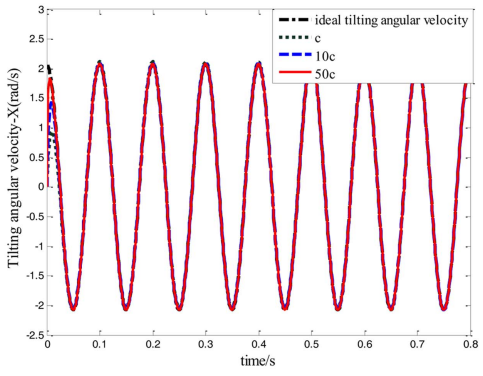

(c) Dynamic response of tilting velocity

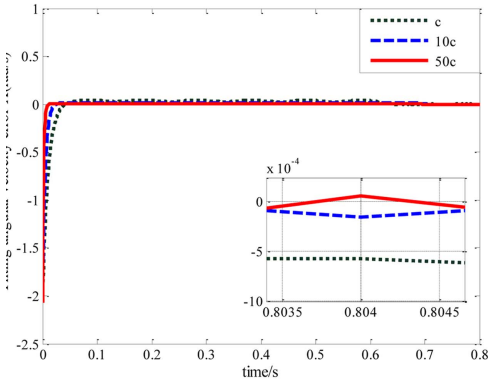

(d) Tracking error of tilting angular velocity

Fig. 7. (Color online) The effect of parameters of the proposed method (harmonic signal).

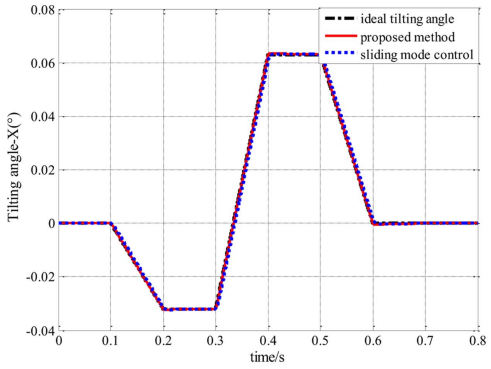

(a) Dynamic response of tilting angle

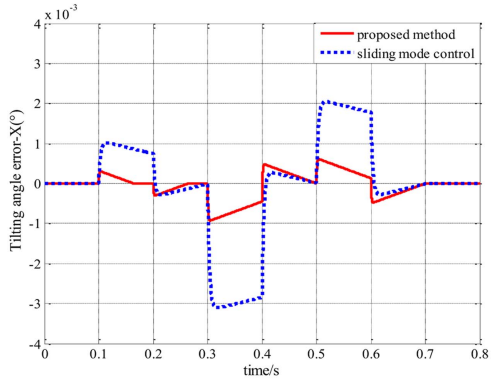

(b) Tracking error of tilting angle

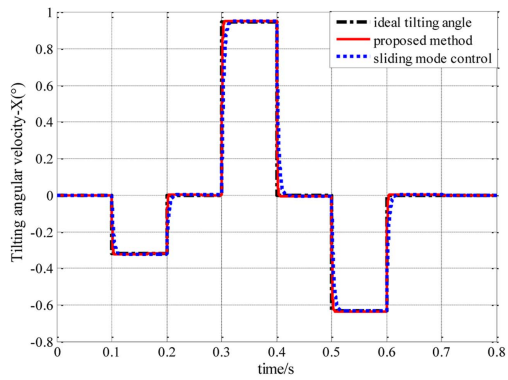

(c) Dynamic response of tilting angle velocity

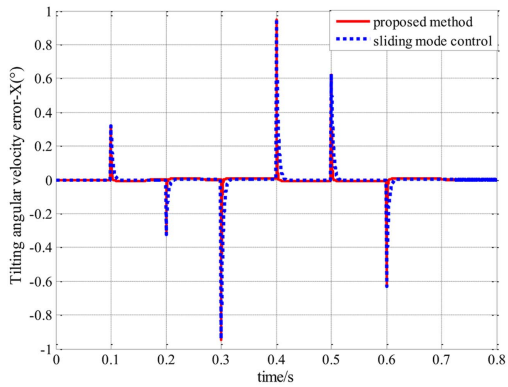

(d) Tracking error of tilting angle velocity

Fig. 8. (Color online) Step tracking performance of SMC with ESO and classic SMC.

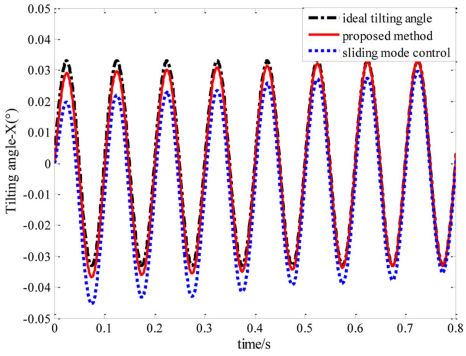

(a) Dynamic response of tilting angle

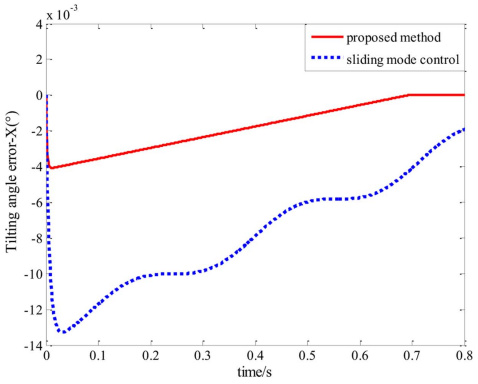

(b) tilting angle error

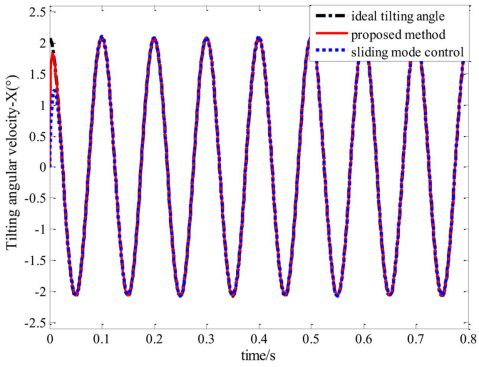

(c) Dynamic response of tilting velocity

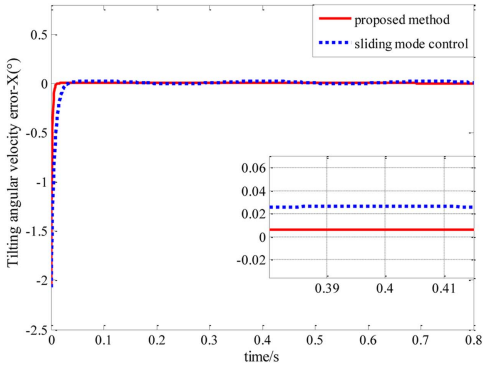

(d) Tracking error of tilting angular velocity

Fig. 9. (Color online) Harmonic tracking performance of SMC with ESO and classic SMC.

in Fig. 8 and Fig. 9. Where the black dashed dot line, the blue dotted ones and the red solid ones are the reference input, the results of the SMC and that of the proposed SMC with ESO, respectively.

Fig. 8 illustrates the step tracking performance of SMC with ESO and classic SMC for the same step tilting angle or tilting angular velocity. We can find out from Fig. 8(a) and (c) that both the classic SMC and SMC with ESO can track step tilting angle or tilting angular velocity stably. From Fig. 8(b), it is found out that the steady error of SMC with ESO is near $3\times10^{-6}(^\circ)$ while that of classic SMC is $6\times10^{-3}(^\circ)$. At the same time, we can find out from Fig. 8(d) that the state error of tilting angular velocity for SMC with ESO is same as that of classic SMC approximately.

Fig. 9 illustrates the harmonic tracking performance of SMC with ESO and classic SMC for the same harmonic tilting angle or tilting angular velocity. It is found out from Fig. 9(a) and (c) that both SMC with ESO and classic SMC can track harmonic tilting angle or tilting angular velocity stably, but the classic SMC has phase delay with respect to the inputting reference signal and its regulation time is longer than that of SMC with ESO. We can also find out from Fig. 9(b) that the state error of tilting angle for classic SMC is near 0.02°, and that of the proposed SMC with ESO is near $1\times10^{-5}(^\circ)$. At the same time, we can find out from Fig. 9(d) that the state error of tilting angular velocity for classic SMC is larger than that for SMC with ESO by about $0.02^\circ/s$.

Therefore, we can draw a conclusion that the proposed SMC with ESO can make the rotor track the inputting signal with high precision and fast response.

4.2. Experimental Tests

To verify the control performance of SMC with ESO on tracking the tilting angle and tilting angular velocity having step form, Fig. 10 is the tested response when the rotor's tilting angle around X-axis is set as ramp signal in case that the rotor's rotary speed is 2000 rpm. Fig. 10(a) illustrates the result of tilting angle, where the expected tilting angle is represented by dot dash line and the tested tracking response is represented by solid line, respectively. It is found out that SMC with ESO can make the rotor track the tilting angle stably; the tracking error is 0.001° (about 1.59 % of expected tilting angle). The tracking response of the tilting angular velocity obtained by derivation of rotor's tilting angles are illustrated in Fig. 10(b), where the dot dash lines represent the expected tilting angular velocity and solid ones represent the tested tilting angular velocity. From Fig. 10(b), it is found out that SMC with ESO can also make the rotor track the

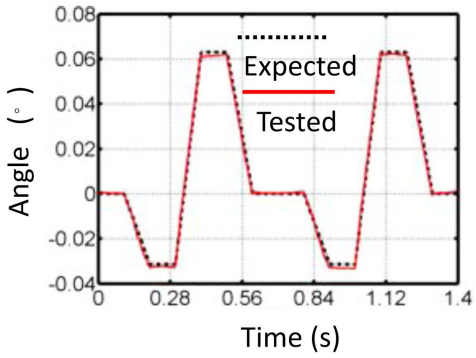

(a) Tracking of step tilting angle

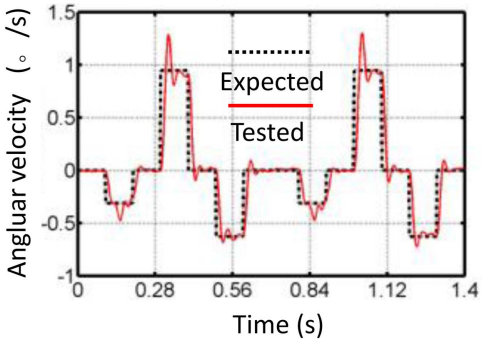

(b) Tracking of step tilting angular velocity

Fig. 10. (Color online) Tested step tracking performance of SMC with ESO.

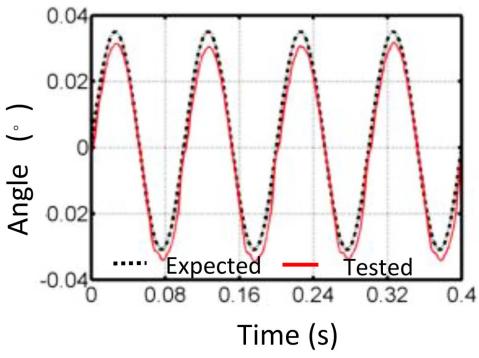

(a) Tracking of harmonic tilting angle

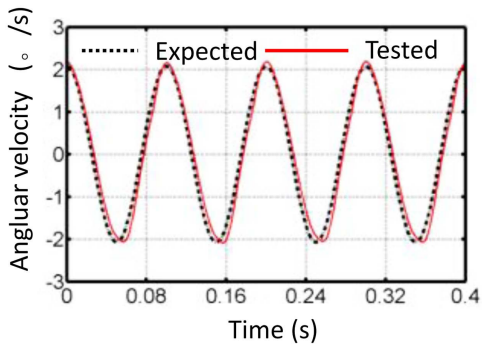

(b) Tracking of harmonic tilting angular velocity

Fig. 11. (Color online) Tested harmonic tracking performance of SMC with ESO.

tilting angular velocity stably. The step response of the velocity 0.945º/s becomes 0º/s at 0.4 s indicate that the rising time of the step response is 0.02s, the peak time is 0.25s, the overshoot is 10.42 % and the regulating time is 0.32s (5 % error zone). These results depicted in Fig.10 indicate that SMC with ESO has high tilting angle tracking accuracy, short regulating time, small overshoot and good dynamic performance to track the step signal of tilting angular velocity.

To verify the control performance of SMC with ESO on tracking the tilting angle and tilting angular velocity having harmonic form, the tested responses are illustrated in Fig. 11 when the tilting angle around X-axis is set as harmonic signal in case that the rotor's rotary speed is 2000 rpm. Fig. 11(a) illustrates the tracking of the rotor's tilting angle around X-axis, where the dot dash line represents the expected tilting angle, the solid line presents the tested response of the tilting angle. From Fig. 11(a), it is found out the peak value of the tracked tilting angle around X-axis is 6.664×10^{-2} º, which is about 1.007 times of the expected values, and the mean value is -1.406×10^{-3} º. The tracking of the tilting angular velocity by SMC with ESO are illustrated in Fig. 11(b), the solid lines represent the tested results of tracking rotor's tilting angular velocity and the dot dash line presents the expected tilting angular velocity. we can find out that SMC with ESO can make the rotor track the harmonic signal of tilting angular velocity stably, the peak value is 4.273 º/s, which is about 1.032 times of the expected values, and the mean error of tracking the rotor's tilting angular velocity around Y-axis is 2.304×10^{-2} º/s. From these results illustrated in Fig. 11.

Fig. 11, we can draw a conclusion that SMC with ESO can make the rotor track the harmonic signals of tilting angle or tilting angular velocity and the related amplitude errors for this harmonic tracking are very small.

5. Conclusion

The Vernier-gimballing MSFW can generate a 1-DOF rotary torque and a 2-DOF tilting torque, thus it has the potential to fulfill the requirements of both precision and maneuvers for spacecraft. For a novel Vernier-gimballing MSFW with a conical MB and a Lorentz MB, the

characteristics of Vernier-gimballing is analyzed and the coupling torque is pointed out as the main problem of the high-precision tilting control.

Considering the coupling torque and the nonlinear magnetic torque generated by conical MB and Lorentz MB respectively, the rotor's dynamic model is constructed, the ESO combined with feedback linearization is proposed originally to estimate this coupling torques, which are hard to model accurately and affect seriously the accuracies of tilting control and outputting torque. To transform the standard system into an integral chain linear one, the feedback linearization based on differential geometry theory is introduced by taking the gyroscopic coupling moment and the current of the Lorentz MB as new virtue inputting. A linear ESO to estimate the coupling torque and its gains are designed reasonably to achieve high precision observation, a SMC with ESO having good compensation and robust performances is proposed to improve the system's robustness, and the stability of the closed-loop system is proved based on Lyapunov stability theory. To verify the rightness and validity of the proposed SMC with ESO, series of simulation and experimental tests are done and these results indicate that this proposed control method can improve the system's tracking accuracy and dynamic performance significantly.

Acknowledgment

This work was supported by Ningbo Nature Science Foundation (Grant No. 2021J011), Beijing Municipal Natural Science Foundation (Grant No. 4222048), and National Natural Science Foundation of China (Grant No. 62073010, 52075017).

References

[1] J.G., Bitterly, Flywheel Technology: Past, Present, and 21st Century Projections, IEEE Aero. El. Sys. Mag. **13**, 13 (1998).
[2] R. Misra, R. Wisniewski, and A. Zuyev, Aerospace **9**, 444 (2022).
[3] P. Silvestrin, Annu. Rev. Control **29**, 247 (2005).
[4] H. M. Liu, H. L. Gao, S. P. Guo, and H. Cai, IEEE Access. **9**, 34475 (2021).
[5] K. R. Rajagopal and K. K. Sivadasan, J. Appl. Phys. **91**, 6994 (2002).
[6] J. Q. Tang, Y. Wang, B. Liu, and X. F. Zhao, T I Meas. Control **41**, 2465 (2019).
[7] C. T. Yu, Y. M. Sun, H. C. Wang, F. Shi, and Y. Chen, J. Mech. Sci. Technol. **33**, 4681 (2019).
[8] J. Q. Tang, X. F. Zhao, Y. Wang, and X. Cui, Proc. I Mech. Eng. I-J Syst. **233**, 1017 (2019).
[9] J. Q. Tang, C. Wang, and B. Xiang, J. Magnetics **18**, 1 (2013).
[10] J. Q. Tang, B. Xiang, and C. Wang, ISA Trans. **58**, 509 (2015).
[11] J. Q. Tang, Z. J. Peng, B. Liu, and K. Wang, IEEE T Ind. Electron. 64, 2972 (2017).
[12] T. Wen and J. C. Fang, Acta Astronaut. **79**, 131 (2012).
[13] L. Lin and T. Gau, IEEE T Contr. Syst. Tech. **5**, 417 (1997).
[14] S. Darbandi, M. Behzad, H. Salarieh, and H. Mehdigholi, IEEE-ASME T Mech. **19**, 1323 (2014).
[15] L. Dong and S. You, ISA Trans. **53**, 1410 (2014).
[16] M. Kang, J. Lyou, and J. Lee, Mechatronics **20**, 171 (2010).
[17] J. H. Lee, P. E. Allaire, G. Tao, and J. A. Decker, IEEE T Contr. Syst. Techn. **11**, 128 (2003).
[18] T. R. Grochmal and A. F. Lynch, IEEE T Contr. Syst. Techn. **15**, 1112 (2007).
[19] Y. Yu, Z. Yang, C. Han, and H. Liu, IEEE T Ind. Electron. **64**, 6528 (2017).
[20] J. Han, IEEE T Ind. Electron. **56**, 900 (2009).
[21] D. Xu, H. Zhou, and Q. Zhang, Int. Conf. Mech. Control, IEEE, Jinzhou, Peoples R China (2014) pp 1402-1406.
[22] K. Li, Z. Deng, C. Liu, and J. Zhou, IEEE Int. Conf. Electr. Mach. Syst., Hangzhou, Peoples R China (2014) pp 1661-1666.
[23] Z. Pu, R. Yuan, J. Yi, and X. Tan, IEEE T Ind. Electron. **62**, 5858 (2015).
[24] C. Chen and H. Qi, J. Harbin Inst. Tech. **25**, 48 (1993).